A novel wavelets method for cancelling time-varying interference in NQR signal detection

Weihang Shao, Jamie Barras, Panagiotis Kosmas

PII: S0165-1684(18)30283-4
DOI: https://doi.org/10.1016/j.sigpro.2018.08.016
Reference: SIGPRO 6908

To appear in: *Signal Processing*

Received date: 20 February 2018
Revised date: 26 August 2018
Accepted date: 31 August 2018

Please cite this article as: Weihang Shao, Jamie Barras, Panagiotis Kosmas, A novel wavelets method for cancelling time-varying interference in NQR signal detection, *Signal Processing* (2018), doi: https://doi.org/10.1016/j.sigpro.2018.08.016

HIGHLIGHTS

- The proposed method is a novel wavelets algorithm which effectively cancels strong and time-varying (nonstationary) interference, despite of a possible strong overlap between the interference and signal of interest, facilitating a valid detection of signal of interest.
- The proposed method uses an extended Gabor-Morlet wavelets basis to approximate interference with complicated time-varying properties. The proposed method utilizes our well designed cost function to strategically extract the interference components out from NQR data precisely without distorting the signal of interest, which is beyond normal wavelets methods such as standard wavelets denoising methods.
- The proposed method outperforms general Fourier analysis and the related frequency selective methods and general adaptive filtering methods on interference cancellation.

A novel wavelets method for cancelling time-varying interference in NQR signal detection

Weihang Shao,[1] Jamie Barras,[1] and Panagiotis Kosmas[1]

[1]*Department of Informatics, King's College London*[*]

(Dated: September 4, 2018)

Abstract

Interference cancelation is a very important aspect of Nuclear Quadrupole Resonance (NQR) signal detection, and can become really difficult when the interference is considerably time-varying. We propose a novel wavelets method to effectively remove (or reduce) time-varying interference in the data and facilitate a valid detection of the NQR signal. The proposed algorithm uses an extended Gabor-Morlet wavelets basis to approximate interference with complicated time-varying properties. The proposed algorithm utilizes our well designed cost function to extract the interference components out from NQR data strategically. Mathematical derivations and numerical results from both simulated and measured data demonstrate that the proposed algorithm can precisely cancel strong time-varying interference without distorting signal of interest improving NQR detection, even when interference and signal of interest are severely overlapped. The proposed algorithm is beyond normal wavelets methods such as standard wavelets denoising methods, and exhibits better performance than normal Fourier analysis and related frequency selective methods and adaptive filtering methods.

[*] This work has been supported by Find a Better Way (FABW) UK, under Project AQUAREOS.

Emails:

weihang.shao@kcl.ac.uk (or picard314@hotmail.com),

jamie.barras@kcl.ac.uk,

panagiotis.kosmas@kcl.ac.uk.

I. INTRODUCTION

Nuclear quadrupole resonance (NQR) signal detection is a useful approach for identifying the presence (or absence) of quadrupolar nuclei substances [1]. This approach has become popular, especially in pharmaceutical monitoring, landmine searching, and oil drilling, because medicine such as narcotics, explosives such as trinitrotoluen (TNT), and petroleum components have their unique NQR signal features/parameters including eigenfrequency and decay time [2–4].

In NQR detection systems, signals can be excited by a specially structured sequence of electromagnetic pulses and recorded by a spectrometer during the time intervals of pulses. The whole system is well designed and is able to work continuously. However, the NQR signal decays quickly with time, while the spectrometer's relaxation time for each recording cycle is long. As a result, the spectrometer's efficiency at recording the NQR response is quite low. To acquire sufficiently long data in each recording cycle, an "echo train" technique can be applied to the spectrometer in order to extract more NQR signal information [5, 6]. During each echo of the recorded data, the NQR signal returns to its initial phase and almost retrieves its original intensity.

Successful signal processing algorithms are an important component of NQR signal detection. If noise and interference are limited, the presence of the NQR signal can be precisely identified by estimating the parameters of the NQR signal based on least square or maximum likelihood theory [7]. Parameter estimation methods can also work for the cases of relatively low signal to noise ratio [8, 9]. However, NQR target responses are not only weak compared to noise, but are further corrupted by strong radio interference which obscures the useful signal response. An easy and very practical method for NQR data processing is to sum each echo, as NQR signal is deterministic and of equal phase among the echoes, and is therefore added coherently, as opposed to stochastic noise and interference. This method is useful for increasing the signal to noise ratio as well as suppressing interference to some extent. However, the efficacy of this method is still limited in practice as data collection time is usually prohibitively long in reality, especially in applications such as humanitarian demining and security checking.

Radio interference is the most challenging source of clutter in NQR detection and is very difficult to remove from the acquired signals. Possible sources of interference include NQR sample impurities and background signals due to radio transmission, and the resulting interference can have strong signal components overlapping with the NQR signal. In many practical applications, interference can also be nonstationary, with time-varying amplitude, frequency, or phase.

Advanced signal processing methods are therefore required to remove this complex interference without distorting the signal of interest.

Amongst traditional techniques to extract/cancel interference signal, adaptive filtering is very popular and useful [10]. However, it requires precise knowledge of the interference properties as reference. In a complex, time-varying environment of NQR application, one should use an additional channel for measuring background interference during data acquisition to acquire synchronous reference information of interference, which is not easy as dealing with gain and phase differences [11] between channels, as well as the instrument operation are challenging. Besides, a representative numerical test (see the Appendix) suggests that normal adaptive filtering methods, even if under almost ideal conditions, does not match the currently proposed method when the interference and the signal of interest is highly overlapped.

To cancel interference, we have proposed an approach [12] referring to the matching pursuit [13] and compressed sensing [14] frameworks. In this approach, Fourier basis is implemented, and the novelty includes the use of a cost function, the specific stop condition, and the effective combination with ETAML [8] algorithm to accomplish the two steps, the first interference cancellation and the second NQR detection, in detecting NQR signal polluted by strong and complex interference [12]. Using cost function (which one can understand is corresponding to the use of measurement matrix in compressed sensing) can achieve better performance compared to finding maximum inner product in matching pursuit, since it can more precisely estimate the frequency of each interference's component, in which case we can prove that our approach effectively cancels interference without distorting signal of interest. Although this approach is very effective in cancelling stationary and slowly time-varying interference in NQR detection applications, however, it cannot account for nonstationary interference, as using Fourier basis can only produce a time average spectrum without details of its time variations.

To deal with commonly encountered nonstationary interference, this paper propose a novel method based on the foundation of our previous work (Ref.[12]) introducing time-frequency analysis with wavelets basis and a corresponding well-designed cost function to track, capture, and then remove time-varying frequency components. The algorithm's first step is coined as the wavelets-based interference cancelation (WIC) algorithm. After cancelling interference by our WIC algorithm, we choose the previously proposed approximate maximum likelihood (AML) [7] method to finally identify the presence (or absence) of the NQR signal. We refer to this two-step algorithm as WICAML.

The remainder of the paper is structured as follows. The theory of the WICAML algorithm is introduced in the next section. In Section III, we apply the WICAML algorithm to both simulated data and experimental data to demonstrate its excellent performance. The last section summarizes the main results.

II. THE THEORY OF THE WICAML ALGORITHM

A. The data model

Considering an echo train detection system, the NQR signal which consists of total d components can be well modelled for the mth echo as [8]

$$y^m(t) = \sum_{k=1}^{d} \alpha_k e^{-\frac{t+m\mu}{T_k^e}} e^{-\frac{|t-t_{sp}|}{T_k^*}+j2\pi\check{f}_k t}, \tag{1}$$

where $j=\sqrt{-1}$, $t=t_0,...,t_{N-1}$ is the N points echo sampling time with the symmetric center to be t_{sp}, $\mu = 2t_{sp}$ is the echo spacing, α_k, T_k^e, T_k^*, and $\check{f}_k$ are the amplitude, echo train decay time, damping time, and frequency of the kth component, respectively. Any data z which contains the NQR signal can be divided into three parts: NQR signal y, noise n, and interference r, that is,

$$z^m(t) = y^m(t) + n^m(t) + r^m(t), \tag{2}$$

for the mth echo. As discussed in the Introduction, each echo contains coherent NQR signals and incoherent noise and interference. By adding all the echoes together, the signal to noise ratio increases, and interference is also partially suppressed. The models of summed signal and data are:

$$\begin{aligned} y(t) &= \sum_m y^m(t) \simeq \sum_{k=1}^{d} A_k e^{-\frac{|t-t_{sp}|}{T_k^*}+j2\pi\check{f}_k t}, \\ z(t) &= \sum_m z^m(t) = y(t) + n(t) + r(t), \end{aligned} \tag{3}$$

where $A_k=\sum_m \alpha_k$. The approximation from Eq. (1) to Eq. (3) is based on the fact "$T_k^e \gg \mu$". We rewrite the data in vector form.

$$\mathbf{Z}_N = \mathbf{Y}_N + \mathbf{N}_N + \mathbf{R}_N, \tag{4}$$

where $\mathbf{N}_N$ and $\mathbf{R}_N$ are the summed noise and interference parts, respectively. The signal part $\mathbf{Y}_N$ satisfies

$$\mathbf{Y}_N = [y(t_0) \quad y(t_1) \quad ... \quad y(t_{N-1})]^{\mathrm{T}} = \mathbb{Q}_N \mathbf{A}, \tag{5}$$

where $(.)^{\mathrm{T}}$ denotes the transpose, $\mathbf{A}$ and $\mathbb{Q}_N$ are the amplitude vector and the phase matrix respectively given by,

$$\mathbf{A} = [A_1 \quad A_2 \quad ... \quad A_d]^{\mathrm{T}}, \tag{6}$$

and

$$\mathbb{Q}_N = \begin{pmatrix} e^{-\frac{|t_0-t_{sp}|}{T_1^*}+j2\pi\check{f}_1 t_0} & e^{-\frac{|t_0-t_{sp}|}{T_2^*}+j2\pi\check{f}_2 t_0} & ... & e^{-\frac{|t_0-t_{sp}|}{T_d^*}+j2\pi\check{f}_d t_0} \\ e^{-\frac{|t_1-t_{sp}|}{T_1^*}+j2\pi\check{f}_1 t_1} & e^{-\frac{|t_1-t_{sp}|}{T_2^*}+j2\pi\check{f}_2 t_1} & ... & e^{-\frac{|t_1-t_{sp}|}{T_d^*}+j2\pi\check{f}_d t_1} \\ ... & ... & ... & ... \\ e^{-\frac{|t_{N-1}-t_{sp}|}{T_1^*}+j2\pi\check{f}_1 t_{N-1}} & e^{-\frac{|t_{N-1}-t_{sp}|}{T_2^*}+j2\pi\check{f}_2 t_{N-1}} & ... & e^{-\frac{|t_{N-1}-t_{sp}|}{T_d^*}+j2\pi\check{f}_d t_{N-1}} \end{pmatrix}. \tag{7}$$

B. NQR signal identification based on approximate maximum likelihood

As we know, in the absence of interference, the approximate maximum likelihood (AML) algorithm [7] is a very useful method for detecting signal of interest masked by noise. We apply AML subsequently after our WIC cancels the interference. Applying other methods such as spectrum analysis and neural network [15] instead of AML is also possible, which is our future work. The AML algorithm estimates the parameters A_k, $\check{f}_k$, and T_k^* in Eq. (3) in the NQR signal model, and then identifies the existence of NQR signal. To do that, the amplitudes vector $\mathbf{A}$ in Eq. (6) is estimated as

$$\hat{\mathbf{A}} = \mathbb{Q}_N^{\dagger}\mathbf{Z}_N, \tag{8}$$

where $(.)^{\dagger}$ denotes the Moore-Penrose pseudo-inverse. Then, the likelihood function for $\check{f}_k$ and T_k^* can be written as

$$L(\check{f}_k, T_k^*) = \mathbf{Z}_N^{\mathrm{H}}\mathbb{Q}_N\mathbb{Q}_N^{\dagger}\mathbf{Z}_N, \tag{9}$$

where $(.)^{\mathrm{H}}$ denotes the conjugate transpose. As $\hat{A}_k$ are functions of $\check{f}_k$ and T_k^*, estimating the parameters A_k, $\check{f}_k$, and T_k^* is equal to finding the $\check{f}_k$ and T_k^* values which satisfy $|L|=\max(|L|)$.

The search ranges for $\check{f}_k$ and T_k^* must cover all possible values of $\check{f}$ and T^* based on prior knowledge of NQR theory [16]. In particular,

$$\check{f}_k = a_k - b_k\mathrm{Temp}, \tag{10}$$

where Temp is the environment temperature, and a_k and b_k are coefficients which are determined by the studied substance, respectively. If Temp has an average value Temp_0 with an uncertainty

ΔT, we have

$$\check{f}_k \in [a_k - b_k \mathrm{Temp}_0 - b_k \Delta T, a_k - b_k \mathrm{Temp}_0 + b_k \Delta T], \tag{11}$$

which are called NQR bands.

Once the estimated parameters $\hat{\check{f}}_k$ and $\hat{T}_k^*$ are acquired, they can be substituted into the AML test statistic [17]

$$T(\mathbf{Z}_N) = (2N-1)\frac{\mathbf{Z}_N^{\mathrm{H}} \mathbb{Q}_N \mathbb{Q}_N^{\dagger} \mathbf{Z}_N}{\mathbf{Z}_N^{\mathrm{H}} \mathbf{Z}_N - \mathbf{Z}_N^{\mathrm{H}} \mathbb{Q}_N \mathbb{Q}_N^{\dagger} \mathbf{Z}_N}. \tag{12}$$

By predetermining a threshold value γ, the NQR signal is deemed present if and only if $T(\mathbf{Z}_N)>\gamma$, and otherwise not. To reduce false alarms, an effective detection algorithm should produce large $T(\mathbf{Z}_N)$ values when the NQR signal is present, and small ones otherwise.

The AML algorithm is very useful when interference in the data is limited. However, its performance degrades if interference becomes very strong, time-varying, and is very close to the NQR signal's frequency. To overcome some of these limitations, a variant of the AML algorithm known as FSAML has also been reported [18]. The FSAML algorithm is a combination of AML and a frequency selective (FS) method. As a way of interference cancelation, this FS method selects the frequency components inside the NQR bands for the data by performing a Discrete Fourier transformation (DFT), and excludes the other frequency components. This is achieved by dividing the NQR bands in a vector of J subbands, $[f_{s1} \quad f_{s2} \quad ... \quad f_{sJ}]$. Then, doing a DFT for $\mathbf{Z}_N$ and $\mathbb{Q}_N$ yields

$$\begin{gathered}\left(\widetilde{\mathbf{Z}}_J, \widetilde{\mathbb{Q}}_J\right) = \mathbb{V}_J\left(\mathbf{Z}_N, \mathbb{Q}_N\right), \\ \mathbb{V}_J = \begin{pmatrix} 1 & e^{-j2\pi f_{s1}/f_s} & .. & e^{-j2\pi(N-1)f_{s1}/f_s} \\ 1 & e^{-j2\pi f_{s2}/f_s} & .. & e^{-j2\pi(N-1)f_{s2}/f_s} \\ .. & .. & .. & .. \\ 1 & e^{-j2\pi f_{sJ}/f_s} & .. & e^{-j2\pi(N-1)f_{sJ}/f_s} \end{pmatrix},\end{gathered} \tag{13}$$

where f_s is the sampling frequency. By combining this method with AML, Eqs.(9) and (12) become,

$$\begin{aligned}\widetilde{L}(\check{f}_k, T_k^*) &= \widetilde{\mathbf{Z}}_J^{\mathrm{H}} \widetilde{\mathbb{Q}}_J \widetilde{\mathbb{Q}}_J^{\dagger} \widetilde{\mathbf{Z}}_J, \\ \widetilde{T}(\widetilde{\mathbf{Z}}_J) &= (2J-1)\frac{\widetilde{\mathbf{Z}}_J^{\mathrm{H}} \widetilde{\mathbb{Q}}_J \widetilde{\mathbb{Q}}_J^{\dagger} \widetilde{\mathbf{Z}}_J}{\widetilde{\mathbf{Z}}_J^{\mathrm{H}} \widetilde{\mathbf{Z}}_J - \widetilde{\mathbf{Z}}_J^{\mathrm{H}} \widetilde{\mathbb{Q}}_J \widetilde{\mathbb{Q}}_J^{\dagger} \widetilde{\mathbf{Z}}_J}.\end{aligned} \tag{14}$$

C. The WIC method

1. *Modelling interference with wavelets*

We formally assume that the central frequencies of interference are all located outside the NQR bands. As NQR bands are very narrow, this assumption covers almost all sources of interference [12]. Interference signals with their center frequencies confined only inside the NQR bands is not a common situation and is outside the scope of this paper. However, the interference and NQR signal, or their subspaces, can be highly overlapped. The proposed method therefore considers interference centered at frequencies inside the interval "$\left[-\frac{f_s}{2}, \frac{f_s}{2}\right]$-NQR bands", marked as C_I, where $\left[-\frac{f_s}{2}, \frac{f_s}{2}\right]$ should be the entire frequency band of complex digital data sampled at frequency f_s. To cancel interference in the NQR data, we propose to select a suitable basis to approximate the interference and then subtract it. Considering that interference (its amplitude or frequency) is time-varying, we choose wavelets basis, in particular that of complex Gabor-Morlet form [19]:

$$\phi(f, \tau, d, t) = e^{j2\pi f(t-\tau)} e^{-\frac{(t-\tau)^2}{2d^2}}, \tag{15}$$

where t is time, f is frequency, τ is time translation, and d denotes the time width factor of this function. We note that, while Gabor-Morlet are amongst the simplest wavelet transforms to model complex-valued data, complex forms of other popular wavelets such as Haar [20] and Daubechies [21] may also be considered as the basis for our WIC algorithm.

The chosen basis in discrete form can be,

$$\left\{\phi_{k_1k_2k_3}(\mathbf{t}) = e^{j2\pi f_{k_1}(\mathbf{t}-\tau_{k_2})} .* e^{-\frac{(\mathbf{t}-\tau_{k_2}).*(\mathbf{t}-\tau_{k_2})}{2d_{k_3}^2}}\right\}, \tag{16}$$

where $\mathbf{t}=[t_0, t_1, ..., t_{N-1}]^{\mathrm{T}}$ is the time vector, $.*$ denotes element by element multiplication, and $k_1 \in \{1, 2, ..., K_1\}$, $k_2 \in \{1, 2, ..., K_2\}$, and $k_3 \in \{1, 2, ..., K_3\}$ are the element counts of $\{\phi_{k_1k_2k_3}(\mathbf{t})\}$ set, respectively. Please note that Eq.(16), termed WIC basis, is an extended Gabor-Morlet wavelets basis. Unlike general Gabor-Morlet wavelets basis, the time width factor d_{k_3} is not fixed in Eq.(16). Moreover, f_{k_1} and τ_{k_2} must be discretizations of the whole interference frequency and time intervals C_I and $[t_{\mathrm{inf}}, t_{\mathrm{sup}}]$ ($t_{\mathrm{inf}} \leq t_0$ and $t_{\mathrm{sup}} \geq t_{N-1}$), respectively, unless the time/frequency distribution of interference is known a priori so that one may shrink the range of f_{k_1} or τ_{k_2}. The choice of d_{k_3} depends on specific interference properties, which will be discussed further in the next subsection.

To use WIC basis expansion effectively, we need to find a linear combination of WIC basis that can approximate well the true interference. To this end, we first introduce the cost function

of $\phi_{k_1k_2k_3}$. Note that $\left|\phi_{k_1k_2k_3}\right|$ is a Gaussian function of t and its main intensity concentrates within $\tau_{k_2} - 3d_{k_3} \leq t \leq \tau_{k_2} + 3d_{k_3}$. From $\mathbf{t}$ and NQR data $\mathbf{Z}_N$, we respectively select all the elements which are inside the time interval $[\max(\tau_{k_2} - 3d_{k_3}, t_0), \min(\tau_{k_2} + 3d_{k_3}, t_{N-1})]$, and make them become new vectors $\mathbf{t}_{k_1k_2k_3}$ and $\mathbf{Z}_{Nk_1k_2k_3}$.

$$\begin{aligned} \mathbf{t}_{k_1k_2k_3} &= [\mathbf{t}(n_i) \quad \mathbf{t}(n_i+1) \quad \mathbf{t}(n_i+2) \quad ... \quad \mathbf{t}(n_s)], \\ \mathbf{Z}_{Nk_1k_2k_3} &= [\mathbf{Z}_N(n_i) \quad \mathbf{Z}_N(n_i+1) \quad \mathbf{Z}_N(n_i+2) \quad ... \quad \mathbf{Z}_N(n_s)], \end{aligned} \tag{17}$$

where n_i=1 or $\mathbf{t}(n_i-1) < \max(\tau_{k_2} - 3d_{k_3}, t_0) \leq \mathbf{t}(n_i)$, and n_s=N or $\mathbf{t}(n_s) \leq \min(\tau_{k_2} + 3d_{k_3}, t_{N-1}) < \mathbf{t}(n_s+1)$, respectively. Then the cost function of $\phi_{k_1k_2k_3}$ is defined as,

$$\begin{aligned} C(k_1,k_2,k_3) &= \frac{\min\limits_{\beta} \left\| \mathbf{Z}_{Nk_1k_2k_3} - \beta\phi_{k_1k_2k_3}(\mathbf{t}_{k_1k_2k_3}) \right\|_2^2}{\left\| \mathbf{Z}_{Nk_1k_2k_3} \right\|_2^2} \\ &= \frac{\left\| \mathbf{Z}_{Nk_1k_2k_3} - \phi_{k_1k_2k_3}(\mathbf{t}_{k_1k_2k_3})\phi^{\dagger}_{k_1k_2k_3}(\mathbf{t}_{k_1k_2k_3})\mathbf{Z}_{Nk_1k_2k_3} \right\|_2^2}{\mathbf{Z}^{\mathrm{H}}_{Nk_1k_2k_3}\mathbf{Z}_{Nk_1k_2k_3}}. \end{aligned} \tag{18}$$

The role of this cost function is to weigh the importance of component (k_1, k_2, k_3) in data $\mathbf{Z}_N$. The smaller the $C(k_1, k_2, k_3)$ is, the higher is the matching degree of $\phi_{k_1k_2k_3}(\mathbf{t})$ to $\mathbf{Z}_N$, that is, the more important is the component (k_1, k_2, k_3). Then, cancelling interference is based on finding the most important components (which should just correspond to the parts of interference) in data $\mathbf{Z}_N$ and removing them.

2. *Cancelling interference with the WIC method*

To cancel time-varying interference based on our wavelet model, we define herein a spectrum threshold $Th(\mathbf{Z}_N)$. Interference components with spectrum intensities that are higher than $Th(\mathbf{Z}_N)$ are regarded as "important" and will be removed by the proposed algorithm [12, 22]. $Th(\mathbf{Z}_N)$ should be higher than the maximum noise spectrum intensity, or causing noise to be "cancelled/distorted" will degrade the performance of the AML algorithm used after WIC according to numerical tests. It is reasonable to let $Th(\mathbf{Z}_N)$ be close to the maximum noise spectrum intensity in order to maximally cancel interference. However, one has to scan the spectrum of $\mathbf{Z}_N$ to find the exact noise level. An efficient approach is to let $Th(\mathbf{Z}_N)$=$2S(\mathbf{Z}_N)$, where

$$S(\mathbf{Z}_N) = \frac{1}{N}\sum_{k=0}^{N-1}\left|\sum_{n=0}^{N-1}\mathbf{Z}_N(n)e^{-j2\pi\frac{kn}{N}}\right|, \tag{19}$$

denotes the average spectrum of the $\mathbf{Z}_N$. According to our numerical tests, $2S(\mathbf{Z}_N)$ is an efficient and easy to calculate threshold choice, which allows the AML algorithm [7] to handle remaining interference.

The proposed WIC method will keep searching iteratively, referring to the framework of matching pursuit [13], until all the interference components whose spectrum intensities are higher than $Th(\mathbf{Z}_N)$ are found and removed. The component with smallest C, marked as $(k_{1m_1}, k_{2m_1}, k_{3m_1})$, can be removed from data $\mathbf{Z}_N$ based on least-square method,

$$\mathbf{Z}_N^{(1)} = \mathbf{Z}_N - \mathbf{W}_{m_1}\mathbf{W}_{m_1}^{\dagger}\mathbf{Z}_N, \tag{20}$$

where $\mathbf{W}_{m_1}$=$\phi_{k_{1m_1}k_{2m_1}k_{3m_1}}(\mathbf{t})$. For the acquired data $\mathbf{Z}_N^{(1)}$, if there is a frequency component $f_{k_1}\in C_I$ which satisfies

$$\left|\sum_{n=0}^{N-1}\mathbf{Z}_N^{(1)}(n)e^{-j2\pi\frac{nf_{k_1}}{f_s}}\right| > Th(\mathbf{Z}_N). \tag{21}$$

This means that some other important components of the interference will still exist. Then a cost function for $\phi_{k_1k_2k_3}$ is defined as

$$C^{(2)}(k_1,k_2,k_3) = \frac{\left\|\mathbf{Z}_{Nk_1k_2k_3}^{(1)} - \phi_{k_1k_2k_3}(\mathbf{t}_{k_1k_2k_3})\phi_{k_1k_2k_3}^{\dagger}(\mathbf{t}_{k_1k_2k_3})\mathbf{Z}_{Nk_1k_2k_3}^{(1)}\right\|_2^2}{\left(\mathbf{Z}_{Nk_1k_2k_3}^{(1)}\right)^{\mathrm{H}}\mathbf{Z}_{Nk_1k_2k_3}^{(1)}}. \tag{22}$$

where $\mathbf{Z}_{Nk_1k_2k_3}^{(1)}$ is created from $\mathbf{Z}_N^{(1)}$ following the rule of "$\mathbf{Z}_{Nk_1k_2k_3}$ from $\mathbf{Z}_N$". Upon finding the component with smallest $C^{(2)}$, marked as $(k_{1m_2}, k_{2m_2}, k_{3m_2})$, it is apparent that both $(k_{1m_2}, k_{2m_2}, k_{3m_2})$ and $(k_{1m_1}, k_{2m_1}, k_{3m_1})$ are important interference components. They can be removed as following:

$$\mathbf{Z}_N^{(2)} = \mathbf{Z}_N - [\mathbf{W}_{m_1} \quad \mathbf{W}_{m_2}][\mathbf{W}_{m_1} \quad \mathbf{W}_{m_2}]^{\dagger}\mathbf{Z}_N. \tag{23}$$

where $[\mathbf{W}_{m_1} \quad \mathbf{W}_{m_2}]$ is formed by combining the vectors to the corresponding matrix. This process can be performed iteratively to cancel interference, as shown in "Table: Iteration" where $C^{(1)}$ and $\mathbf{Z}_N^{(0)}$ are C and $\mathbf{Z}_N$, respectively.

Table: Iteration

i=0;

while $\left(\left|\sum_{n=0}^{N-1}\mathbf{Z}_N^{(i)}(n)e^{-j2\pi\frac{nf_{k_1}}{f_s}}\right| > Th(\mathbf{Z}_N)\right)$

i=i+1;

$C^{(i)}(k_{1m_i},k_{2m_i},k_{3m_i})$

$= \min\limits_{k_1,k_2,k_3}\left[\frac{\left\|\mathbf{Z}_{Nk_1k_2k_3}^{(i-1)}-\phi_{k_1k_2k_3}(\mathbf{t}_{k_1k_2k_3})\phi_{k_1k_2k_3}^{\dagger}(\mathbf{t}_{k_1k_2k_3})\mathbf{Z}_{Nk_1k_2k_3}^{(i-1)}\right\|_2^2}{\left(\mathbf{Z}_{Nk_1k_2k_3}^{(i-1)}\right)^{\mathrm{H}}\mathbf{Z}_{Nk_1k_2k_3}^{(i-1)}}\right]$;

$\mathbf{W}_{m_i}$=$\phi_{k_{1m_i}k_{2m_i}k_{3m_i}}(\mathbf{t})$;

$\mathbf{Z}_N^{(i)} = \mathbf{Z}_N - [\mathbf{W}_{m_1} \quad ... \quad \mathbf{W}_{m_i}][\mathbf{W}_{m_1} \quad ... \quad \mathbf{W}_{m_i}]^{\dagger}\mathbf{Z}_N$;

end

Finally, the interference-canceled data $\mathbf{Z}_N^{(l)}$

$$\begin{aligned}\mathbf{Z}_N^{(l)} &= \mathbf{Z}_N \\ &\quad - [\mathbf{W}_{m_1} \quad \mathbf{W}_{m_2} \quad ... \quad \mathbf{W}_{m_l}][\mathbf{W}_{m_1} \quad \mathbf{W}_{m_2} \quad ... \quad \mathbf{W}_{m_l}]^{\dagger}\mathbf{Z}_N,\end{aligned} \tag{24}$$

is acquired, which satisfies $\left|\sum_{n=0}^{N-1}\mathbf{Z}_N^{(l)}(n)e^{-j2\pi\frac{nf_{k_1}}{f_s}}\right| \leq Th(\mathbf{Z}_N)$, for $\forall f_{k_1}\in C_I$, where l denotes the number of removed interference components.

As a result, the interference is effectively suppressed and its remnant parts can be treated as "parts of noise". As the iteration stops when the rest interference and the noise are of comparable intensity, the WICAML algorithm becomes the classical AML algorithm when applied to data without interference and with white noise.

D. Analysis on the properties of the WIC basis

We first note that if fixing d=+∞, the WIC basis (see Eq.(16)) are just equivalent to our Fourier basis in our recently proposed FT based interference cancelation (FIC) method [12] (see also the Introduction). Although the WIC basis cannot be absolutely orthogonal as the Fourier basis, it has a definite advantage over Fourier basis for processing time-varying interference. Below we discuss important properties of our WIC basis that ensure that the signal of interest remains intact after cancelling interference.

We start by noting that the spectrum of the WIC basis is

$$\Phi_{k_1k_2k_3}(f) = \int_{-\infty}^{+\infty} \phi_{k_1k_2k_3}(t)e^{-j2\pi ft}dt = \sqrt{2\pi}d_{k_3}e^{-2\pi^2(f_{k_1}-f)^2d_{k_3}^2}, \tag{25}$$

which is also a Gaussian function. $\Phi_{k_1k_2k_3}(f)$ has no sidelobe, and tends to be $\delta(f - f_{k_1})$ (the spectrum of Fourier basis) when $d_{k_3}\to+\infty$. So, if the value of d_{k_3} is large enough, canceling interference using Eq. (24) causes limited distortion to other frequency components in the data, such as the NQR signal. The inner product for the WIC basis yields,

$$\begin{aligned}
|<\phi_2,\phi_1>| &= \left|\int_{-\infty}^{+\infty}\phi_2^*\phi_1 dt\right| \\
&= \left|\left[\int_{-\infty}^{+\infty} e^{-\frac{d_1^2+d_2^2}{2d_1^2d_2^2}\left(t-\frac{j2\pi f_1d_1^2d_2^2-j2\pi f_2d_1^2d_2^2+d_2^2\tau_1+d_1^2\tau_2}{d_1^2+d_2^2}\right)^2}dt\right]\right. \\
&\left.\times e^{-\frac{4\pi^2(f_1-f_2)^2d_1^2d_2^2+(\tau_1-\tau_2)^2+4\pi j(f_1d_1^2+f_2d_2^2)(\tau_1-\tau_2)}{2(d_1^2+d_2^2)}}\right| \\
&= \frac{\sqrt{2\pi}d_1d_2}{\sqrt{d_1^2+d_2^2}}e^{-\frac{4\pi^2(f_1-f_2)^2d_1^2d_2^2+(\tau_1-\tau_2)^2}{2(d_1^2+d_2^2)}},
\end{aligned} \tag{26}$$

where ϕ_1 and ϕ_2 satisfy "$f_1\neq f_2$". Thus, we have $e^{-\frac{4\pi^2(f_1-f_2)^2d_1^2d_2^2+(\tau_1-\tau_2)^2}{2(d_1^2+d_2^2)}} \ll 1$ if d_1 and d_2 are large enough, and further derive that

$$\begin{aligned}
|<\phi_1,\phi_2>| = |<\phi_2,\phi_1>| &\ll \sqrt{2}\,|<\phi_1,\phi_1>|, \\
|<\phi_1,\phi_2>| = |<\phi_2,\phi_1>| &\ll \sqrt{2}\,|<\phi_2,\phi_2>|,
\end{aligned} \tag{27}$$

where $d_1, d_2 > d_1d_2/\sqrt{d_1^2+d_2^2}$ is used. Eq.(27) suggests that ϕ_1 and ϕ_2 are approximately orthogonal. Similarly, considering the time factor of NQR signal, $s_k = e^{-\frac{|t-t_{sp}|}{T_k^*}+j2\pi\check{f}_kt}$, we can also derive

$$\begin{aligned}
&|<\phi_1,s_k>| \le \left|<\phi_1,e^{j2\pi\check{f}_kt}>\right| \ll \sqrt{2}\,|<\phi_1,\phi_1>|, \\
&\left(\lim_{d_1\to+\infty}\left|<\phi_1,e^{j2\pi\check{f}_kt}>\right| = 0\right), \\
&|<\phi_1,s_k>| \ll |<s_k,s_k>| = T_k^*,
\end{aligned} \tag{28}$$

since f_1 is outside NQR bands (i.e. $f_1\neq\check{f}_k$). Please note $|<s_k,s_k>|$ and $|<\phi_1,\phi_1>|$ are comparable since $|<\phi_1,\phi_1>| = \sqrt{\pi}d_1 \sim T_k^*$. Thus, Eq.(28) suggests that ϕ_1 and s_k are approximately orthogonal. Now, for $\mathbf{W}_{m_1}$, $\mathbf{W}_{m_2}$, ..., $\mathbf{W}_{m_l}$ in Eq. (24), we let

$$\begin{aligned}
\mathbb{G} &= \left[\mathbf{W}_{m_1} \quad \mathbf{W}_{m_2} \quad ... \quad \mathbf{W}_{m_l}\right], \\
\mathbb{G}^\dagger &= \left[\mathbf{W}_1^{\mathrm{T}} \quad \mathbf{W}_2^{\mathrm{T}} \quad ... \quad \mathbf{W}_l^{\mathrm{T}}\right]^{\mathrm{T}},
\end{aligned} \tag{29}$$

where $\mathbf{W}_1$, $\mathbf{W}_2$, ...,$\mathbf{W}_l$ are $1\times N$ vectors, and $\mathbf{V}_i=\mathbf{W}_{m_i}\mathbf{W}_i\mathbf{Z}_N$, i=1,2,...,l. Furthermore, if a $\mathbf{W}_{m_i}$ has center frequency f_{k_1}, we count it into group S_{k_1}. We rewrite $\mathbf{W}_{m_i}$ as $\mathbf{W}_{k_1}^{(q)}$ if it is the q-th element in group S_{k_1}, and $\mathbf{V}_i$ becomes $\mathbf{V}_{k_1}^{(q)}$, accordingly. With this notation, $\widetilde{\mathbf{V}}_p=\sum_q \mathbf{V}_{k_1}^{(q)}$ is the p-th component vector of the extracted interference, where p=1,2,...,l' and l' is the number of group S_{k_1}. As we know, the energy of the interference cancelled data $\mathbf{Z}_N^{(l)}$, $E^{(l)}=\left\|\mathbf{Z}_N^{(l)}\right\|_2^2=\left(\mathbf{Z}_N^{(l)}\right)^{\mathrm{H}}\mathbf{Z}_N^{(l)}$, satisfies

$$\begin{aligned} E^{(l)} &= \mathbf{Z}_N^{\mathrm{H}}\mathbf{Z}_N - \left(\mathbb{G}\mathbb{G}^{\dagger}\mathbf{Z}_N\right)^{\mathrm{H}}\mathbb{G}\mathbb{G}^{\dagger}\mathbf{Z}_N \\ &= \mathbf{Z}_N^{\mathrm{H}}\mathbf{Z}_N - \left(\sum_{i=1}^{l}\mathbf{V}_i\right)^{\mathrm{H}}\left(\sum_{i=1}^{l}\mathbf{V}_i\right). \\ &= \mathbf{Z}_N^{\mathrm{H}}\mathbf{Z}_N - \left(\sum_{p=1}^{l'}\widetilde{\mathbf{V}}_p\right)^{\mathrm{H}}\left(\sum_{p=1}^{l'}\widetilde{\mathbf{V}}_p\right). \end{aligned} \tag{30}$$

In fact, from Eq.(27), we have

$$\left|\mathbf{V}_i^{\mathrm{H}}\mathbf{V}_j\right| = \left|\mathbf{Z}_N^{\mathrm{H}}\mathbf{W}_i^{\mathrm{H}}\left(\mathbf{W}_{m_i}^{\mathrm{H}}\mathbf{W}_{m_j}\right)\mathbf{W}_j\mathbf{Z}_N\right| \ll \mathbf{V}_i^{\mathrm{H}}\mathbf{V}_i, \tag{31}$$

if $\mathbf{V}_i$ and $\mathbf{V}_j$ are not in the same group. Then from Eq. (31) we can derive that

$$\left|\widetilde{\mathbf{V}}_p^{\mathrm{H}}\widetilde{\mathbf{V}}_{p'}\right| \ll \widetilde{\mathbf{V}}_p^{\mathrm{H}}\widetilde{\mathbf{V}}_p, \quad p \neq p'. \tag{32}$$

Substituting Eq.(32) into Eq.(30) yields

$$E^{(l)} \simeq \mathbf{Z}_N^{\mathrm{H}}\mathbf{Z}_N - \sum_{p=1}^{l'}\widetilde{\mathbf{V}}_p^{\mathrm{H}}\widetilde{\mathbf{V}}_p, \tag{33}$$

which means that approximately the energy of each interference component does not contain/grab the energy of any other component in $\mathbf{Z}_N$. Besides, as mentioned before, Eq. (25) suggests that each $\mathbf{V}_i$ (or each interference component $\widetilde{\mathbf{V}}_p$) with center frequency f_{k_1} holds limited information of other frequency components in $\mathbf{Z}_N$. Furthermore, similarly to Eq. (31), we also obtain

$$\begin{aligned} \left|\mathbf{V}_i^{\mathrm{H}}\mathbf{Y}_N\right| &\ll \mathbf{V}_i^{\mathrm{H}}\mathbf{V}_i, \\ \left|\mathbf{V}_i^{\mathrm{H}}\mathbf{Y}_N\right| &\ll \mathbf{Y}_N^{\mathrm{H}}\mathbf{Y}_N, \end{aligned} \tag{34}$$

from Eq. (28).

Eqs. (33) and (34) suggest that the NQR signal inside $\mathbf{Z}_N$ can approximately remain intact when using Eq. (24) to cancel interference. This is verified by our results in Figs. 3, 11, 7, and 15 of the next Section, which clearly show that the NQR signal peaks in the frequency domain are almost perfectly restored after interference cancellation by our WIC algorithm. This requires selecting

a proper basis set $\{\phi_{k_1k_2k_3}(\mathbf{t})\}$ in Eq.(16) that can represent the interference signal with minimum redundancy. The selection could be easy if there is prior knowledge of the time-frequency energy distribution of the interference. But if not, our method determines $\{\phi_{k_1k_2k_3}(\mathbf{t})\}$ in Eq.(16) based on a time-frequency plot of the original data $\mathbf{Z}_N$.

In particular, a time-frequency plot can produce "zones" of frequency and time of all interference components (see Figs. 1, 5, 9, and 13 as examples). These zones must be covered by the selected ranges for f_{k_1} and τ_{k_2} in our WIC model. Proper selection on d_{k_3} is especially important, since "$2d_{k_3}$" represents the effective width of a wavelets basis element. By letting the values of $2d_{k_3}$ be close to the time widths of interference regions in the time-frequency plots, the basis elements can fit the time size of interference causing little redundancy in interference cancellation. The process of choosing d_{k_3} is based on the following rules: (1) let the elements of $2d_{k_3}$ correspond to the main time widths of the interference regions; (2) prudently choose smaller values of d_{k_3}, as basis elements with smaller d_{k_3} relatively cause more redundancy; (3) if the time width of an interference region is large (close to the echo's length), it is helpful to accordingly invoke Fourier elements adding $+\infty$ into d_{k_3} congregation, or try some "$2d_{k_3}$ >1 echo length"; (4) in practice, if one is not very sure which set of basis is deemed proper, it is effective to use several "perhaps suitable" sets for respectively calculating $\mathbf{Z}_N^{(l)}$ and then choose the one with minimum l as a final result, as fewer $\mathbf{W}_{m_i}$ in Eq.(24) relatively cause less redundancy.

Apparently, the WIC method is beyond normal wavelets methods such as standard wavelets denoising methods [23]. The extended Gabor-Morlet wavelets basis as well as its proper selections, the well designed cost function, and the referred matching pursuit framework ensure more precise estimations of interference components, and cancelling interference without distorting/cancelling the signal of interest.

III. THE PERFORMANCE OF THE WICAML ALGORITHM

This section presents results from both simulated data and experimental data to test the performance of the WICAML algorithm. NQR detection performance is compared with the previously proposed AML [7], FSAML [18], and FICAML [12] algorithms. Simulated data is produced to resemble our experimental data with sodium nitrite producing the NQR signal of interest, as detailed in Section III-A. The algorithms are then applied to data polluted by different types of time-varying interference, presented in Sections III-B, C, and D.

A. Introduction to our NQR data

Our testbed examines detection of the ^{14}N NQR signal due to sodium nitrite ($NaNO_2$). To acquire experimental data, we prepared two sealed plastic boxes which were both filled with silicone oil and were buried under soil separately. All conditions are the same between the two boxes except for the presence of a piece of solid $NaNO_2$, which is suspended in the silicone oil in only one of the boxes. Signal data in echo train mode is recorded by a spectrometer with a sampling frequency $f_s = \frac{1}{16\mu s}$. Two data sets are acquired for each run/record, one with and one without the NQR signal. The data consists of N=128 sampling points (complex numbers) per echo. For the studied substance under our lab conditions, the NQR signal has only one resonant frequency $\check{f}\simeq$1.0365MHz, and T^* in Eq. (3) is approximately equal to 1.74ms. In addition, b in Eq. (10) is 600Hz/Kelvin, and the lab temperature uncertainty ΔT is about 0.8Kelvin.

In the measurements, we scanned information within the frequency band $\left[f_c - \frac{f_s}{2}, f_c + \frac{f_s}{2}\right]$, and the final modulated data recorded by spectrometer has the frequency band $\left[-\frac{f_s}{2}, \frac{f_s}{2}\right]$, where f_c is the frequency center of signal modulation. In particular, we set $f_c \simeq \check{f}$, so that the modulated NQR band is $[-b\Delta T, +b\Delta T]$ (see Eq. (11)).

In our calculations, the search range for $\check{f}$ is the NQR band with the search step being set as $\frac{b\Delta T}{10}$, which is also for calculating Eq. (13). And the search range of T^* is set to be $[1.74\text{ms} \times 0.01, 1.74\text{ms} \times 10.01]$ which already covers all the possible values of T^* under our lab conditions according to NQR theory [16], with the search step being $\frac{1.74\text{ms}}{100}$. Besides, we let $f_{k_1} \in \left\{-\frac{f_s}{2}, -\frac{f_s}{2} + \frac{f_s}{10N}, ..., -b\Delta T, b\Delta T, b\Delta T + \frac{f_s}{10N}, ..., \frac{f_s}{2}\right\}$, and $\tau_{k_2} \in \{0, 1, ..., 20\} \times \frac{t_{N-1} - t_0 + dt}{20}$, where dt=t_1-t_0, respectively. In order to avoid unnecessary calculation time, if the frequencies and time distribution of interference are known a priori, for example by doing time-frequency analysis, f_{k_1} and τ_{k_2} can simply cover the ranges of those of interference. The above grids we set are fine enough for dealing with general time-varying interference in NQR data. Parallel computing methods and advanced optimum search methods with variable search step (such as conjugate gradient method [24]) can also be applied, in order to speed up the search calculation.

B. Simulated data test I: a general example of time-varying interference

A simulated data set containing 100 Monte Carlo runs is created. In this set, the NQR signal amplitude A in Eq. (3) is 1, and the noise is zero-mean Gaussian white noise with variance D=0.25.

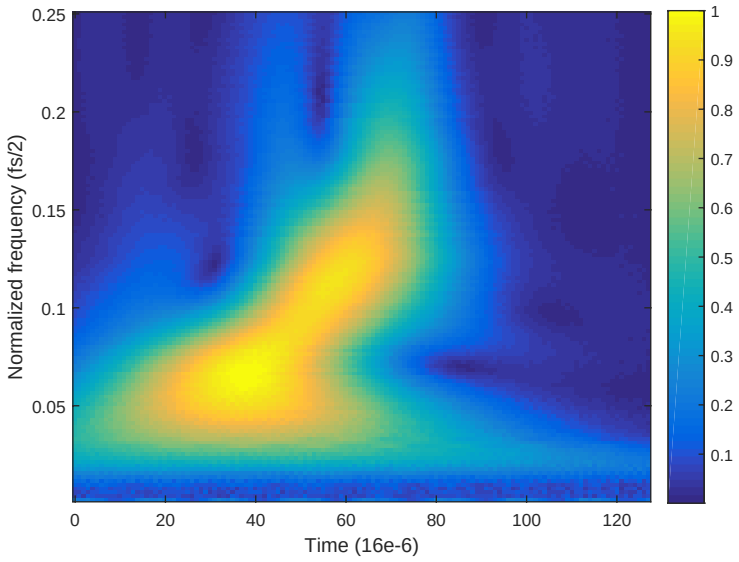

FIG. 1. (Color online) The time-frequency analysis on a run of the original data of simulation test I. It is achieved using Morlet wavelets of 'cmor1-1' in Matlab environment. This figure provides information for choosing proper d_{k_3} as described in the end of Section II. The intensity of the displayed time-frequency information is normalized.

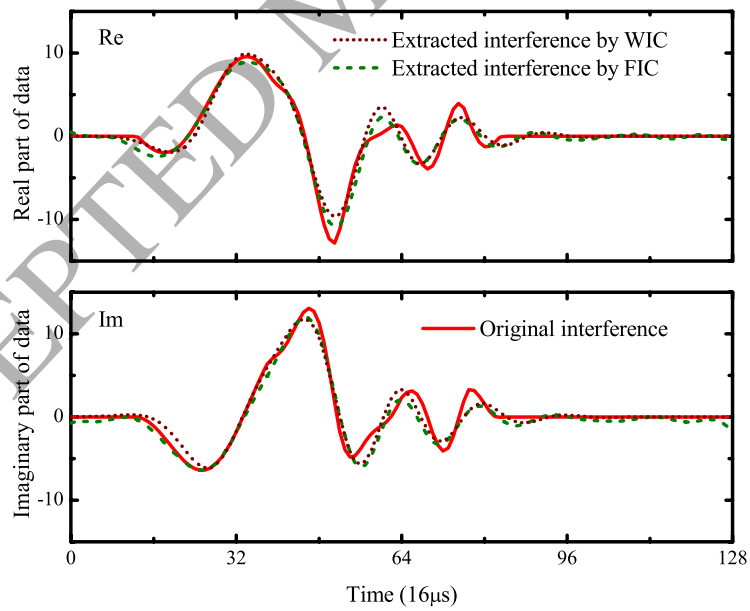

FIG. 2. (Color online) Interference extraction (in the time domain) of a run of the original data in simulation test I respectively by FIC and the proposed WIC methods.

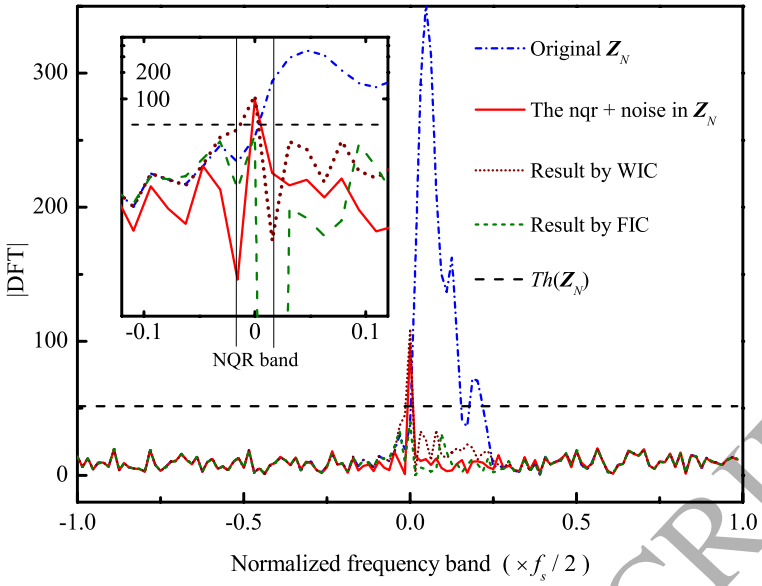

FIG. 3. (Color online) The spectra of a run of the original data and the interference canceled data of simulation test I. "|DFT|" means the absolute value of Discrete Fourier transformation of data. The embedded subgraph zooms in the area around NQR band, with its vertical axis of logarithm to the base 10.

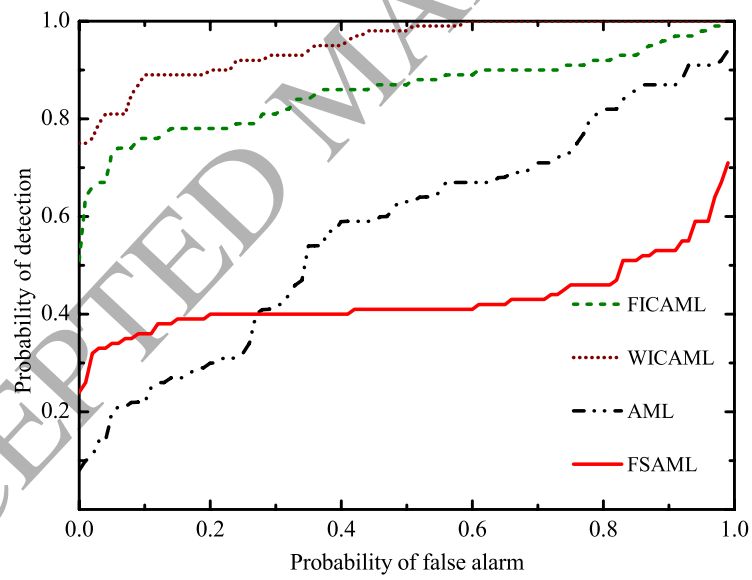

FIG. 4. (Color online) The ROC curves obtained by AML, FSAML, FICAML, and WICAML algorithms. The results are for the simulation test I.

Then the signal to noise ratio,

$$\mathrm{SNR} = 20\lg\left(\frac{\pi}{4}\cdot\frac{A^2}{D}\right), \tag{35}$$

is calculated as 10dB, which is close to that for our experimental data. The interference is described in the following table,

Interference I
$r(t) = \sum_{i=1}^{3} r_i(t)$,
$r_i(t) = 0 \quad (t \le t_{start_i} \quad \text{or} \quad t \ge t_{start_i} + D_i)$,
$r_i(t) = Ar_i \sin\left[\frac{2\pi(t-t_{start_i})}{2D_i}\right] e^{j2\pi f_i(t)t + j\varphi_i}$
$(t_{start_i} < t < t_{start_i} + D_i)$,
where counting i from 1 to 3,
$Ar_i = 10, 9, 8, \quad D_i/(t_{N-1} - t_0 + dt) = 0.4, 0.2, 0.35,$
$t_{start_i}/(t_{N-1} - t_0 + dt) = 0.1, 0.2, 0.3,$
$N^2 f_i(t)/f_s = (3N + 3f_s t), (9N - 2.7 f_s t), (8N - 2.2 f_s t).$

where the initial phases φ_i are all random among the runs. As is mentioned before, time-frequency analysis on the original simulated data is made in prior in a Matlab environment for determining suitable d_{k_3} of WIC basis. As shown in Fig. (1), the result gives the time distribution of all frequency components in the data as well as their duration. Interference is mainly located in the region "Frequency 0.03-0.16 and Time 20-70". We accordingly choose two kinds of d_{k_3}.

d_{k_3} for Interference I
$d_{k_3}/(t_{N-1} - t_0 + dt) \in \{0.25, 0.26, ..., 0.3\}$,
$d_{k_3}/(t_{N-1} - t_0 + dt) \in \{0.2, 0.21, ..., 0.3\}$.

The interference cancelation results are displayed in Figs. 2 and 3 via time- and frequency-domain plots, respectively. As shown in Fig. 2, both the extracted interferences by WIC and FIC are close to the exact interference in the original data $\mathbf{Z}_N$. However, a time-domain plot may be insufficient for judging whether the interference cancellation distorts the signal of interest. On the contrary, the frequency-domain plots of Fig. 3 show that the signal peak is almost restored perfectly after interference cancelation by WIC, while the Fourier analysis based FIC approach does not lead to good performance distorting the NQR signal, as it fails to capture the time variations of the interference signals.

Figure 4 shows the receiver operating characteristic (ROC) curves given by different algorithms.

The WICAML provides reliable detection result while results from the other algorithms are significantly worse. Not unexpectedly, the ROC curves from the pure AML algorithm and its frequency selective variant FSAML suggest poor performance due to the strong interference which has not been cancelled effectively. As this interference is strong in frequencies which are very close to the NQR band, the frequency selection processes within the FSAML algorithm cannot be efficient. FIC is able to precisely cancel interference which even has frequencies very close to NQR band providing strong sidelobe effects inside NQR band, but it can only be suitable for stationary and slowly time-varying interference. Finally, FICAML performs much better than AML and FSAML, but cannot outer-perform WICAML, which can account for time-varying interference more accurately.

C. Simulated data test II: time-varying interference of multiple frequency components

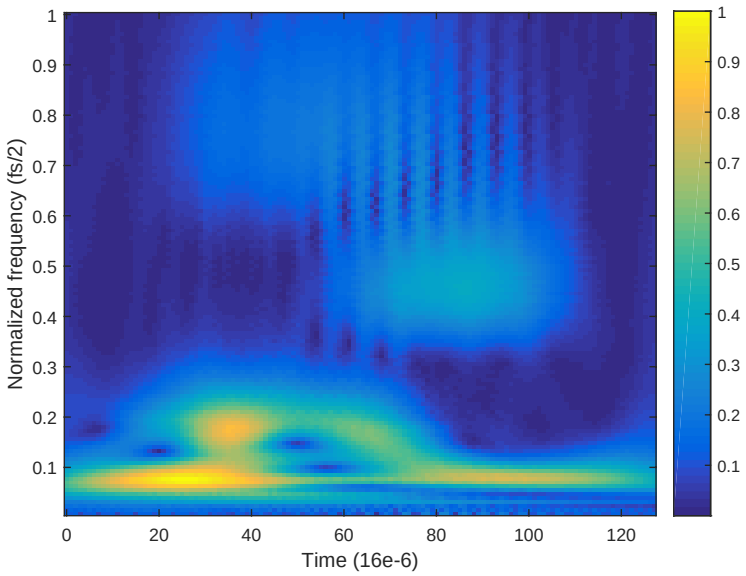

FIG. 5. (Color online) The time-frequency analysis on a run of the original data of simulation test II. It is achieved using Morlet wavelets of 'cmor1-1' in Matlab environment. This figure provides information for choosing proper d_{k_3} as described in the end of Section II. The intensity of the displayed time-frequency information is normalized.

In a complicated practical environment, interference may come from different kinds of sources so that it may contain multiple frequency components. The simulated data in this subsection inherits the NQR signal and the noise in last subsection but adds more interference components

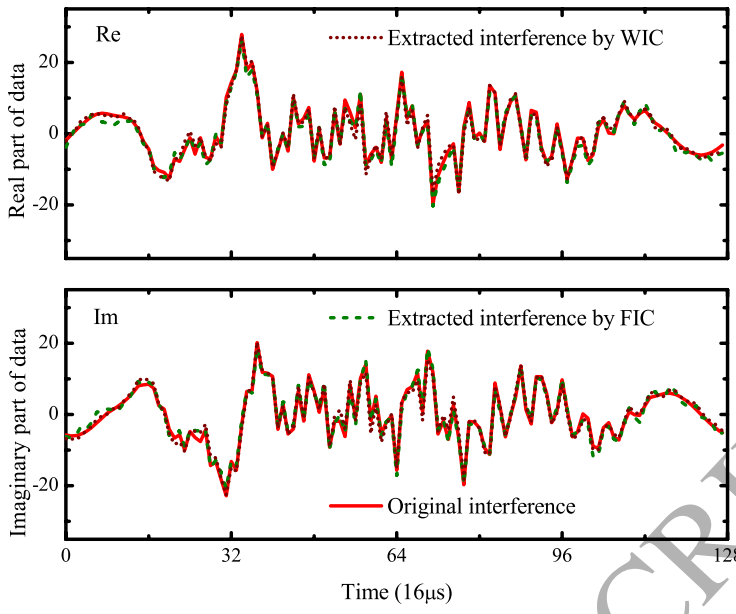

FIG. 6. (Color online) Interference extraction (in the time domain) of a run of the original data in simulation test II respectively by FIC and the proposed WIC methods.

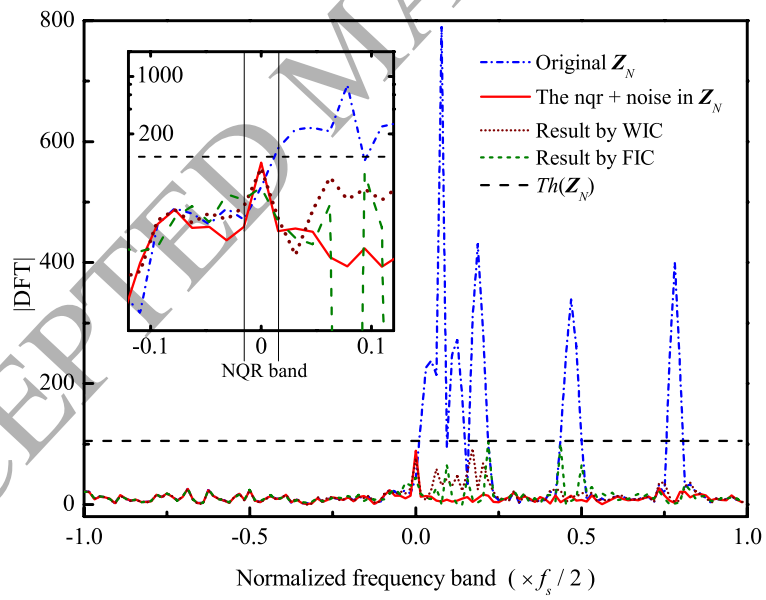

FIG. 7. (Color online) The spectra of a run of the original data and the interference canceled data of simulation test II. "|DFT|" means the absolute value of Discrete Fourier transformation of data. The embedded subgraph zooms in the area around NQR band, with its vertical axis of logarithm to the base 10.

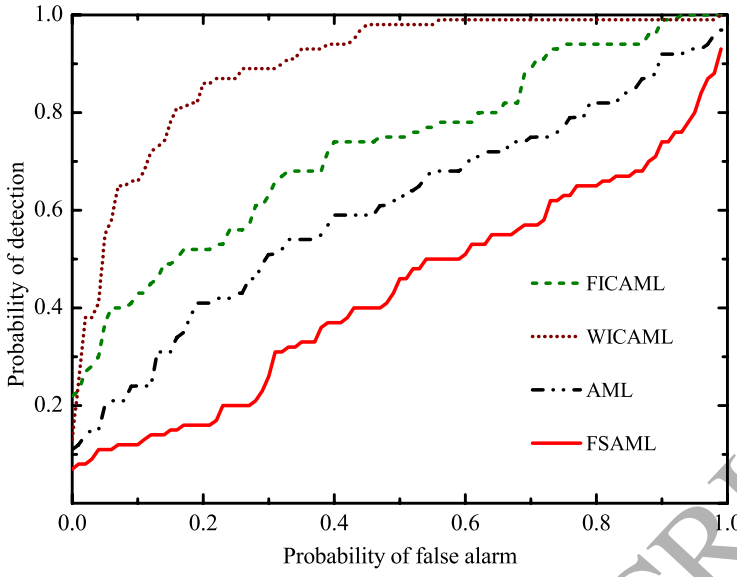

FIG. 8. (Color online) The ROC curves obtained by AML, FSAML, FICAML, and WICAML algorithms. The results are for the simulation test II.

within the frequency spectrum. The simulated interference is shown in the following table,

Interference II

$$r(t) = \sum_{i=1}^{6} r_i(t) + r_{stat}(t),$$
$$r_{stat}(t) = 6e^{j2\pi f_{stat}t + j\varphi_{stat}}, \quad f_{stat} = 5f_s/N,$$
$$r_i(t) = 0 \quad (t \le t_{start_i} \quad \text{or} \quad t \ge t_{start_i} + D_i),$$
$$r_i(t) = Ar_i \sin\left[\frac{2\pi(t - t_{start_i})}{2D_i}\right] e^{j2\pi f_i(t)t + j\varphi_i}$$
$$(t_{start_i} < t < t_{start_i} + D_i),$$

where counting i from 1 to 6,

$$Ar_i = 8, 7, 6, 7, 8, 7,$$
$$D_i/(t_{N-1} - t_0 + dt) = 0.4, 0.2, 0.35, 0.6, 0.5, 0.7,$$
$$t_{start_i}/(t_{N-1} - t_0 + dt) = 0.1, 0.2, 0.3, 0.05, 0.4, 0.1,$$
$$N^2 f_i(t)/f_s = (3N + 3f_s t), (9N - 2.7f_s t),$$
$$(8N - 2.2f_s t), (12N + 7f_s t), (30N - 8f_s t), (50N - 6f_s t).$$

where $r_{stat}(t)$ is a stationary component, and the initial phases φ_{stat} and φ_i are all random among the runs, respectively. The time-frequency information of the data are shown in Fig. 5. Referring to the time widths of interference

region, we choose two kinds of d_{k_3} for calculation shown below:

d_{k_3} for Interference II
$d_{k_3}/(t_{N-1} - t_0 + dt) \in \{0.3, 0.4, +\infty\}$,
$d_{k_3}/(t_{N-1} - t_0 + dt) \in \{0.4, 0.5, +\infty\}$.

WIC's performance is displayed in Figs. 6 and 7, which suggest good performance for this case of interference, which is much more complicated than in the previous subsection. The ROC curves in Fig. 8 confirm that the WICAML can lead to a valid NQR detection in this case.

D. Simulated data test III: time-varying interference of very short period

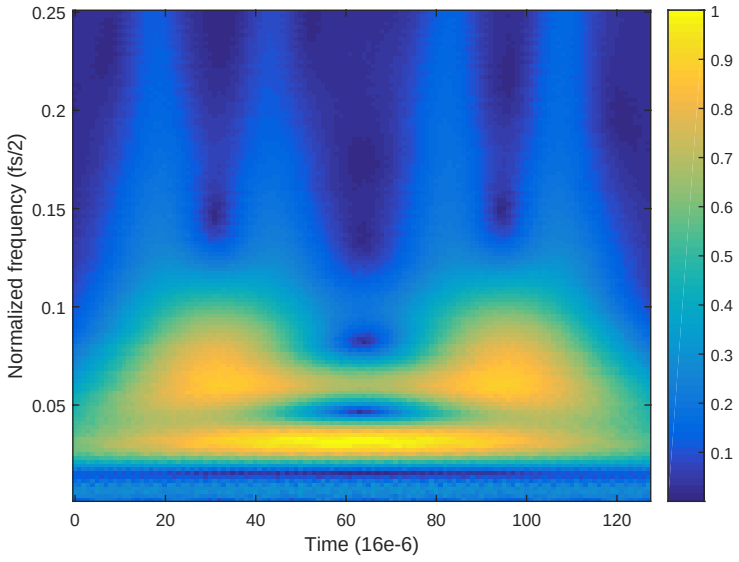

FIG. 9. (Color online) The time-frequency analysis on a run of the original data of simulation test III. It is achieved using Morlet wavelets of 'cmor1-1' in Matlab environment. This figure provides information for choosing proper d_{k_3} as described in the end of Section II. The intensity of the displayed time-frequency information is normalized.

To further explore the performance of the WIC method in dealing with extremely time-varying interference, we have also simulated and tested a case of very short-period interference. The data here has the same NQR signal and noise as before, and the new interference signal is:

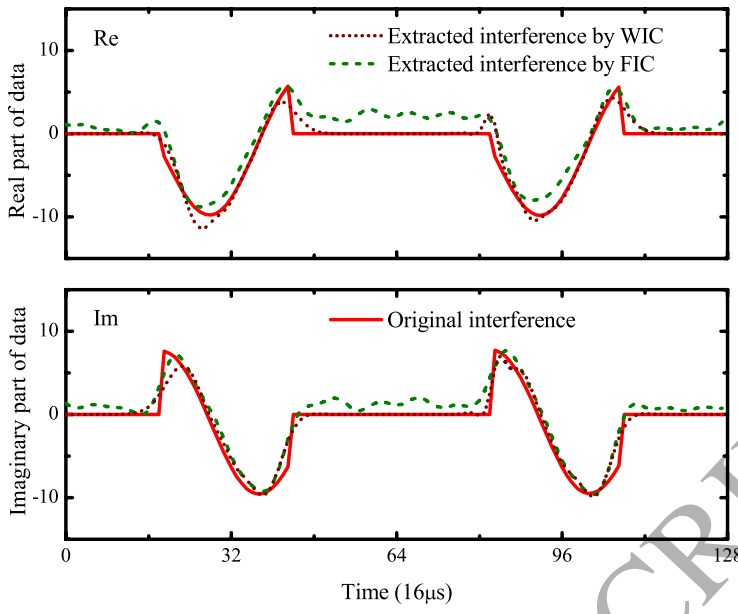

FIG. 10. (Color online) Interference extraction (in the time domain) of a run of the original data in simulation test III respectively by FIC and the proposed WIC methods.

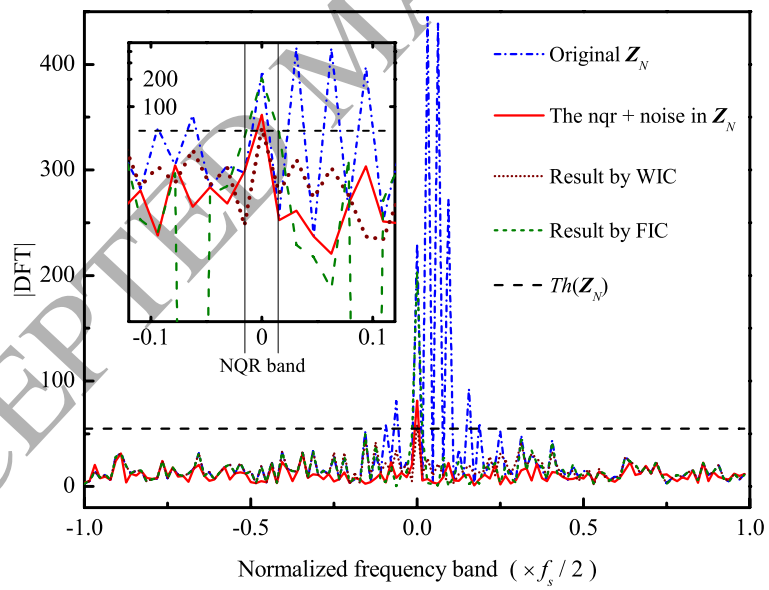

FIG. 11. (Color online) The spectra of a run of the original data and the interference canceled data of simulation test III. "|DFT|" means the absolute value of Discrete Fourier transformation of data. The embedded subgraph zooms in the area around NQR band, with its vertical axis of logarithm to the base 10.

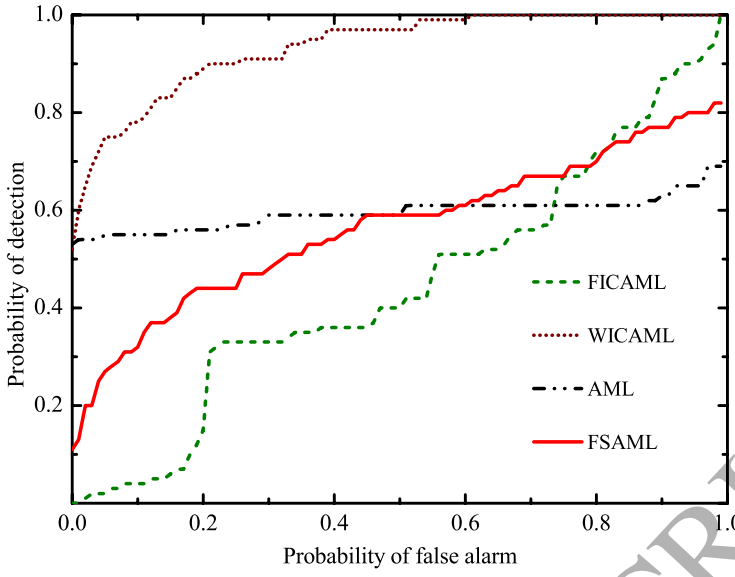

FIG. 12. (Color online) The ROC curves obtained by AML, FSAML, FICAML, and WICAML algorithms. The results are for the simulation test III.

Interference III

$r(t) = 10 \sin\left(\frac{2\pi t}{t_{N-1}-t_0}\right) e^{j2\pi f(t)t + j\varphi}$
if $\frac{t}{t_{N-1}-t_0} \in (0.15, 0.35) \bigcup (0.65, 0.85)$,
$r(t) = 0$
if else.
$N^2 f(t)/f_s = (3N + 3f_s t)$.

where the initial phase φ is random among the runs. As we can see in Fig. 10, the interference in the time domain resembles two pulses. Moreover, the spectrum of this interference looks very complicated and contains very strong sidelobes inside the NQR band (see Fig. 11). The time-frequency analysis is provided in Fig. 9. Referring to the time widths of interference region, we

choose two kinds of d_{k_3} shown in the next table,

d_{k_3} for Interference III
$d_{k_3}/(t_{N-1} - t_0 + dt) \in \{0.05, 0.06, ..., 0.2, +\infty\}$,
$d_{k_3}/(t_{N-1} - t_0 + dt) \in \{0.05, 0.06, ..., 0.1, +\infty\}$.

Figs. 10 and 11 suggest that the interference cancelation by WIC is successful. This is confirmed by the good performance of the WICAML algorithm expressed by the ROC curves shown in Fig. 12. On the contrary, FICAML is very problematic in this case. FICAML is based on FT analysis which inevitably averages the interference effect along the whole data time period as if assuming that interference is always present. Artificial results by FIC can be seen clearly in Fig. 10 (especially the middle part of time), and distort the NQR signal severely (see the NQR peak in Fig. 11). The strong time variations of the interference signal even cause the FICAML to show no advantage over AML.

E. Experimental data test

The experimental data we acquired consists of a total of 100 runs, with an SNR being about 4dB. From the result of time-frequency analysis in Fig. 13, it is clear that the interference frequency spectrum is mainly located very close to the NQR band, and the interference is strong and obviously time-varying. Referring to the time widths of interference region, we let:

d_{k_3} for interference in experimental data
$d_{k_3}/(t_{N-1} - t_0 + dt) \in \{2, +\infty\}$,
$d_{k_3}/(t_{N-1} - t_0 + dt) \in \{2.5, +\infty\}$.

The interference cancelation results and ROC curves are displayed in Figs. 14, 15, and 16, respectively. As in the previous cases, the WICAML algorithm leads to accurate NQR detection and has better performance than Fourier based algorithm FICAML due to the time variation of the interference.

In practice, it is important to test the algorithm's robustness to varying levels of noise. For this reason, we acquired and tested additional experimental datasets with different SNR levels. Our results confirmed that the WICAML algorithm is robust and outer-performs the other three algo-

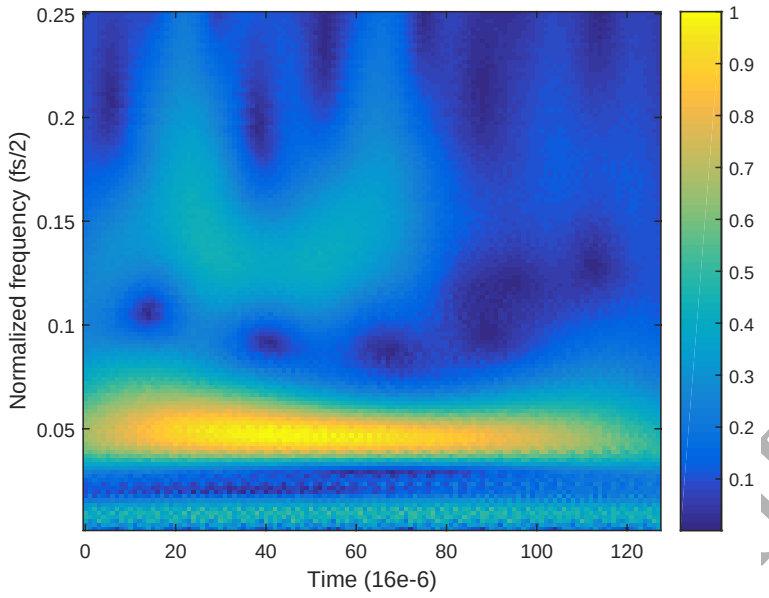

FIG. 13. (Color online) The time-frequency analysis on a run of the original data of the experimental test. It is achieved using Morlet wavelets of 'cmor1-1' in Matlab environment. This figure provides information for choosing proper d_{k_3} as described in the end of Section II. The intensity of the displayed time-frequency information is normalized.

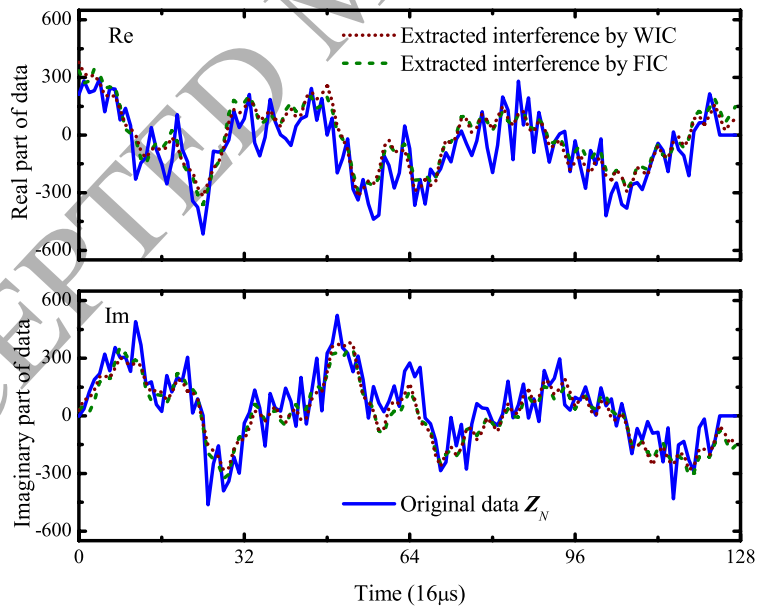

FIG. 14. (Color online) Interference extraction (in the time domain) of a run of the original experimental data respectively by FIC and the proposed WIC methods.

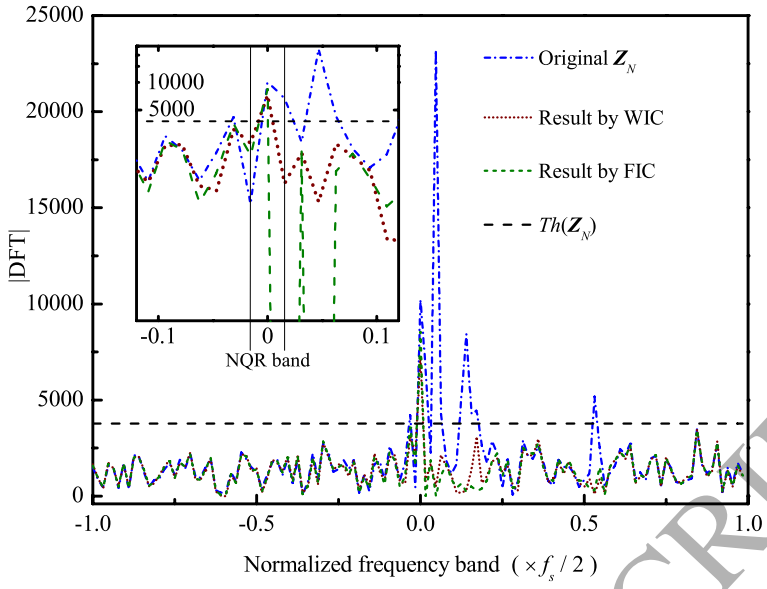

FIG. 15. (Color online) The spectra of a run of the original data and the interference canceled data of the experimental test. "|DFT|" means the absolute value of Discrete Fourier transformation of data. The embedded subgraph zooms in the area around NQR band, with its vertical axis of logarithm to the base 10.

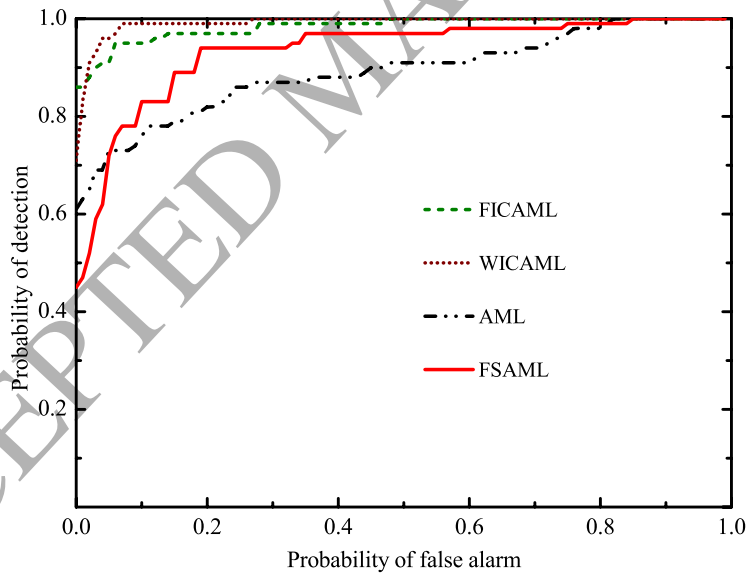

FIG. 16. (Color online) The ROC curves obtained by AML, FSAML, FICAML, and WICAML algorithms. The results are for the experimental test where the SNR is about 4dB.

rithms. Naturally, WICAML's detection performance degrades as the SNR decreases. In relation to Fig. 16, Fig. 17 presents ROC curves for experimental data of lower SNR (about -3dB). These

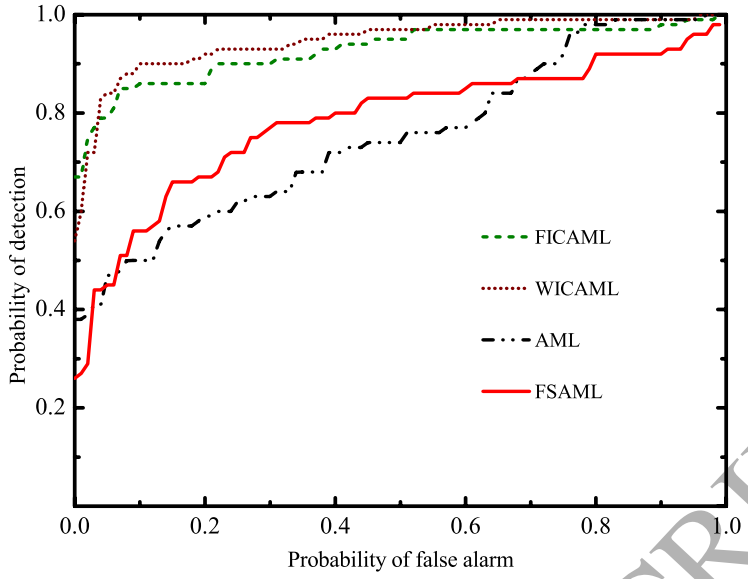

FIG. 17. (Color online) The ROC curves obtained by AML, FSAML, FICAML, and WICAML algorithms. The results are calculated from experimental data of lower signal to noise ratio (about -3dB).

preliminary experimental results suggest that the WICAML algorithm can improve significantly NQR detection in real-life settings dealing with complicated time-varying interference.

IV. CONCLUSION

This paper presents a novel interference cancelation method which can enhance NQR signal detection in situations of strong time-varying interference. The method relies on a wavelets basis expansion but is beyond normal wavelets methods such as standard wavelets denoising methods, which can model and cancel time-varying interference much more effectively than our Fourier based interference cancelation method. Also, we illustrate that the method has advantages over adaptive filtering methods. The method can be coupled with the classical Approximate Maximum Likelihood (AML) algorithm for signal identification, resulting in the formulation of the so-called WICAML algorithm. We note that the AML algorithm deals with the "signal and noise only" case, and its performance is compromised if data are severely polluted by interference. The paper's results show that the WICAML algorithm exhibits excellent performance when applied to simulated data or experimental data which contain complicated time-varying interference. The WIC interference cancellation method could be readily applied to other signal processing areas like radar signal, acoustic signal. etc., under a similar framework, beyond the NQR signal detection problem

studied in this work.

V. APPENDIX

We herein illustrate that normal adaptive filtering methods [10], even if under almost ideal conditions, can not match the proposed algorithm in cancelling interference that is highly overlapped with signal of interest. To do that, we present a simulated case,

Sampling Time (t)	$t = 0, \frac{1}{N}, \frac{2}{N}, ..., \frac{N-1}{N}$, or $t(k) = \frac{k}{N}$, $N = 128$.
Signal of Interest (s)	$s = \exp(j2\pi \times 0.8t + j\phi) \times \exp(-\lvert t - 0.5\rvert / T_d)$, $T_d = 1$, $\phi \in [0, 2\pi]$.
Interference (r)	$r = 0.8\exp(j2\pi \times 2.2t + j\phi_1) + 1.2\exp(j2\pi \times 2.5t + j\phi_2)$. $\phi_1, \phi_2 \in [0, 2\pi]$.
Noise (n)	Gaussian white, zero-mean, variance=0.25.
Reference (r_1)	$r_1 \equiv r$.

In this case, s and r are highly overlapped/correlated (see the dash dot dot line in Fig.19). The signal of interest contains a damping term $\exp(-|t - 0.5|/T_d)$ as an imitation to the NQR signal model (see Eq.(3)). When $T_d \to +\infty$, the signal of interest has the general sinusoidal form. Moreover, we assume that the adaptive detection on background interference performs perfectly which means that the acquired reference interference r_1 is absolutely the same as the exact interference r.

Let $x = s + n + r$ be the data. We first discuss the use of Wienner filter methods [10]. Interference's k-th point can be calculated using a N-order Wienner filter,

$$r_w(k) = \sum_{i=0}^{N-1} w_k(i)x(k-i), \quad k = 0, 1, 2, ..., N-1. \tag{36}$$

where the past $N-1$ points (before k) of s, n, r, and r_1 are the backward continuation of them, and

the Wienner filter coefficients vector $\mathbf{w}_k$ satisfies

$$\begin{pmatrix} R_{xx}(0;k) & R_{xx}(1;k) & .. & R_{xx}(N-1;k) \\ R_{xx}(1;k) & R_{xx}(0;k) & .. & R_{xx}(N-2;k) \\ .. & .. & .. & .. \\ R_{xx}(N-1;k) & R_{xx}(N-2;k) & .. & R_{xx}(0;k) \end{pmatrix} \mathbf{w}_k = \begin{pmatrix} R_{xr}(0) \\ R_{xr}(1) \\ .. \\ R_{xr}(N-1) \end{pmatrix}, \tag{37}$$

where

$$\begin{aligned} R_{xx}(m;k) &= \frac{1}{N}\sum_{i=0}^{N-|m|-1} x(i+k-N+1)x(i+m+k-N+1), \\ R_{xr}(m;k) &= \frac{1}{N}\sum_{i=0}^{N-|m|-1} x(i+k-N+1)r_1(i+m+k-N+1), \end{aligned} \tag{38}$$

are the autocorrelation of x and the cross-correlation between x and r_1, respectively.

We have also considered the use of Kalman filter [25] for getting the interference estimation $\hat{r}$. The Kalman equation set contains two parts, (a) the priori estimation part,

$$\begin{aligned} \hat{r}_0(k) &= F_k \hat{r}(k-1), \\ \hat{P}_0(k) &= F_k \hat{P}(k-1) F_k^* + Q_k, \end{aligned} \tag{39}$$

where $\hat{P}$ is the interference estimation error covariance, $\hat{r}_0$ and $\hat{P}_0$ are the priori interference estimation and estimation error covariances, $F_k = \frac{r(k)}{r(k-1)} + \Delta_k$ is the state-transition coefficient assumed to be known already under an Gaussian uncertainty of $\Delta_k \sim N(0, \sigma^2)$, and Q_k is the process error covariance due to Δ_k, respectively; (b) the posteriori estimation part,

$$\begin{aligned} K_k &= \frac{\hat{P}_0(k) H_k^*}{H_k \hat{P}_0(k) H_k^* + S_k}, \\ \hat{r}(k) &= \hat{r}_0(k) + K_k \left(z(k) - H_k \hat{r}_0(k)\right), \\ \hat{P}(k) &= \left(1 - K_k H_k\right) \hat{P}_0(k), \end{aligned} \tag{40}$$

where $H_k = 1$ is the observation coefficient, $z(k) = x(k)$ is the observation data, K_k is the Kalman gain, and S_k is the observation error covariance, respectively. We ideally assume that the initial values of $\hat{r}(k)$ and $\hat{P}(k)$ are $r(k=-1)$ and 0, respectively, and a good knowledge of both Q_k and

S_k has been acquired. Indeed, if $\sigma = 0$, $\hat{r} \equiv r$; or if $S_k \equiv 0$, $\hat{r} \equiv x \equiv r$. However, we cannot avoid errors in practice and σ is set to be 0.01 (very small compared to $r(k)/r(k-1)$) for the following simulation. In the simulation, we let Q_k and S_k be

$$Q_k \equiv \frac{1}{N-1}\sum_{i=0}^{N-1}\left|\Delta_i r(i-1) - \frac{1}{N}\sum_{l=0}^{N-1}\Delta_l r(l-1)\right|^2,$$

$$S_k \equiv \frac{1}{N-1}\sum_{i=0}^{N-1}\left|x(i)+n(i) - \frac{1}{N}\sum_{l=0}^{N-1}(x(l)+n(l))\right|^2,$$

respectively.

Please note that data from NQR spectrometer is complex and equations related to Wienner and Kalman filters can be applied to the real and imagination parts of the data, respectively.

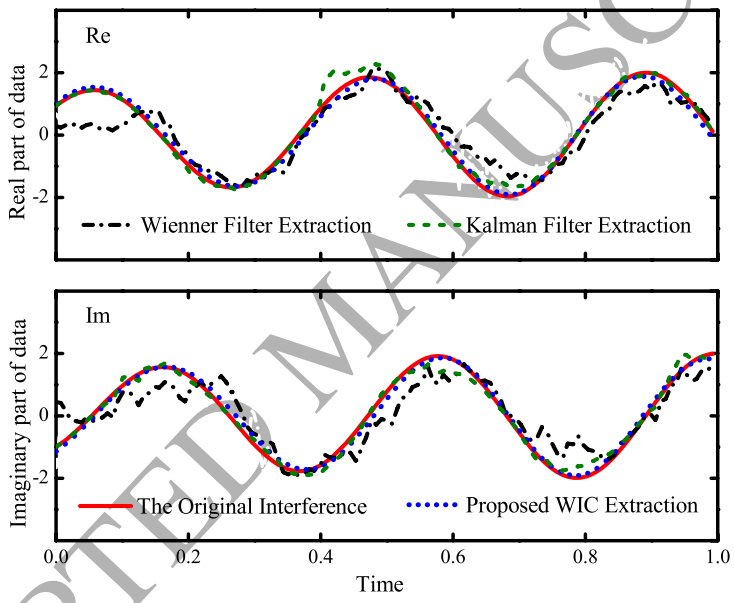

FIG. 18. (Color online) Interference extraction (shown in the time domain) respectively by Wienner filter, Kalman filter, and the proposed WIC methods.

It is clearly shown in Figs. 18 and 19 that both the (adaptive) Wienner and Kalman filters have no better performance than the proposed WIC method, as in the time domain only WIC extracts interference that close to the exact one, and in the frequency domain only WIC restores the peak of signal of interest after doing interference cancellation. When the interference and the signal of interest are highly overlapped/correlated, general filters can not effectively divide them from each other.

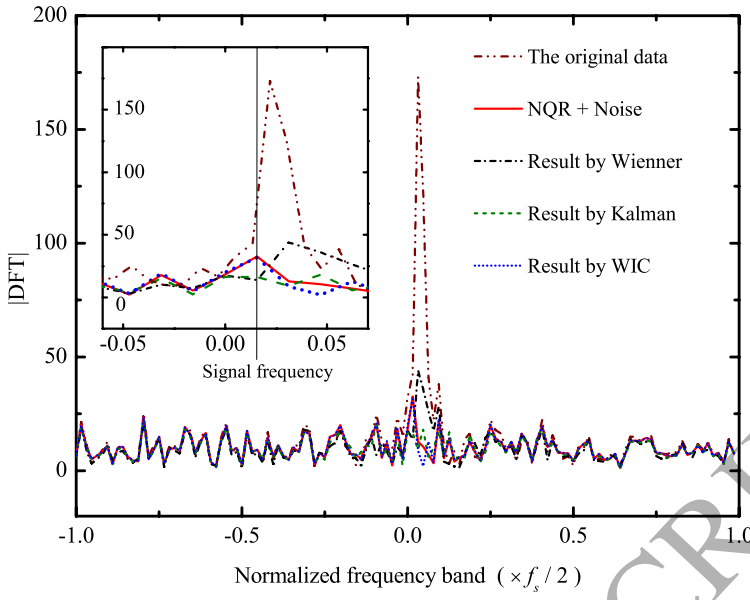

FIG. 19. (Color online) Data (show in the frequency domain) after interference cancellation respectively by Wienner filter, Kalman filter, and the proposed WIC methods. "|DFT|" means the absolute value of Discrete Fourier transformation of data. The embedded subgraph zooms in the area around NQR band.

ACKNOWLEDGMENT

This work has been supported by Find a Better Way (FABW) UK, under Project AQUAREOS.

[1] J. A. S. Smith, "Nuclear quadrupole resonance spectroscopy," *J. Chem. Educ.*, vol. 48, no. 1, pp. 39–48, 1971.

[2] N. R. Butt, E. Gudmundson, and A. Jakobsson, "An overview of NQR signal detection algorithms," in *Magnetic Resonance Detection of Explosives and Illicit Materials*, ser. NATO Science for Peace and Security Series B: Physics and Biophysics, T. Apih, B. Rameev, G. Mozzhukhin, and J. Barras, Eds. Springer, 2013, pp. 19–34.

[3] J. Barras, D. Murnane, K. Althoefer, S. Assi, M. D. Rowe, I. Poplett, G. Kyriakidou, and J. A. S. Smith, "Nitrogen-14 nuclear quadrupole resonance spectroscopy: a promising new analytical methodology for medicines authentication and counterfeit antimalarial analysis," *Anal. Chem.*, vol. 84, pp. 2746–2753, 2013.

[4] J. Barras, K. Althoefer, M. D. Rowe, I. Poplett, and J. A. S. Smith, "The emerging field of nuclear qudrupole resonance-based medicines authentication," *Appl. Magn. Reson.*, vol. 43, pp. 511–529, 2012.

[5] M. D. Rowe and J. A. S. Smith, "Mine detection by nuclear quadrupole resonance," *in Proc. EUREL Int. Conf. on the Detection of Abandoned Land Mines*, pp. 62–66, Oct. 1996.

[6] A. Gregorovič and T. Apih, "Relaxation during spin-lock spin-echo pulse sequence in n 14 nuclear quadrupole resonance," *J. Chem. Phys.*, vol. 129, p. 214504, 2008.

[7] A. Jakobsson, M. Mossberg, M. D. Rowe, and J. A. S. Smith, "Exploiting temperature dependency in the detection of nqr signals," *IEEE Trans. Signal Proces.*, vol. 54, no. 5, pp. 1610–1616, 2006.

[8] S. D. Somasundaram, A. Jakobsson, J. A. S. Smith, and K. Althoefer, "Exploiting spin echo decay in the detection of nuclear quadrupole resonance signals," *IEEE Trans. Geosc. Remote Sensing*, vol. 45, pp. 925–933, 2007.

[9] S. D. Somasundaram, A. Jakobsson, J. Smith, and K. Althoefer, "Robust nuclear quadrupole resonance signal detection allowing for amplitude uncertainties," *IEEE Trans. Signal Proces.*, vol. 56, no. 3, pp. 887–894, 2008.

[10] S. Haykin, *Adaptive Filter Theory*. Tom Robbins, 2002.

[11] J. Li, P. Stoica, and W. Wang, "On robust capon beamforming and diagonal loading," *IEEE Trans. Signal Proces.*, vol. 51, no. 7, pp. 1702–1715, 2003.

[12] W. Shao, J. Barras, K. Althoefer, and P. Kosmas, "Detecting nqr signals severely polluted by interference," *Signal Processing*, vol. 138, pp. 256–264, 2017.

[13] S. G. Mallat and Z. Zhang, "Matching pursuits with time-frequency dictionaries," *IEEE Trans. Signal Proces.*, vol. 41, pp. 3397–3415, 1993.

[14] D. L. Donoho, "Compressed sensing," *IEEE Trans. Inform. Theory*, vol. 52, no. 4, pp. 1289–1306, 2006.

[15] W. Shao, J. Barras, and P. Kosmas, "Detection of extremely weak nqr signals using stochastic resonance and neural network theories," *Signal Processing*, vol. 142, pp. 96–103, 2018.

[16] S. D. Somasundaram, "Advanced signal processing algorithms based on novel nuclear quadrupole resonance models for the detection of explosives," Ph.D. dissertation, King's College London, 2007.

[17] S. M. Kay, *Fundamentals of Statistical Signal Processing, Volume II: Detection Theory*. Englewood Cliffs, NJ: Prentice-Hall, 1998.

[18] A. Jakobsson, M. Mossberg, M. D. Rowe, and J. A. S. Smith, "Frequency-selective detection of nuclear quadrupole resonance signals," *IEEE Trans. Geosc. Remote Sensing*, vol. 43, no. 11, pp. 2659–2665, 2005.

[19] T. Anthony, *Computational Signal Processing with Wavelets*. Birkhäuser, Springer, 1998.

[20] A. Haar, "Zur theorie der orthogonalen funktionensysteme," *Math. Annal.*, vol. 69, no. 3, pp. 331–371, 1910.

[21] I. Daubechies, *Ten Lectures on Wavelets*. Society for Industrial and Applied Mathematics, 1992.

[22] J. A. Högbom, "Aperture synthesis with a non-regular distribution of interferometer baselines," *Astronomy and Astrophysics Supplement*, vol. 15, pp. 417–426, 1974.

[23] A. Boggess and F. J. Narcowich, *A First Course in Wavelets with Fourier Analysis*. Wiley, 2011.

[24] M. R. Hestenes and E. Stiefel, "Methods of conjugate gradients for solving linear systems," *Journal of Research of the National Bureau of Standards*, vol. 49, pp. 409–436, 1952.

[25] R. E. Kalman, "A new approach to linear filtering and prediction problems," *J. Basic Eng*, vol. 82, pp. 35–45, 1960.